Chemical Science

ROYAL SOCIETY OF CHEMISTRY

EDGE ARTICLE

View Article Online
View Journal | View Issue

Cite this: *Chem. Sci.*, 2021, **12**, 9500

All publication charges for this article have been paid for by the Royal Society of Chemistry

Received 2nd March 2021
Accepted 14th June 2021

DOI: 10.1039/d1sc01220g

rsc.li/chemical-science

Boosting cancer therapy efficiency *via* photoinduced radical production†

Zhiyong Liu,‡ Mengsi Wu,‡ Minbo Lan * and Weian Zhang *

Current cancer therapy has been restricted by the hypoxic microenvironment of tumors, especially for strongly oxygen-dependent photodynamic therapy. To defeat tumor hypoxia, an oxygen-irrelevant radical nanogenerator, **PI/FBC**, is developed by the co-assembly of iodized polymer **PI** and NIR photosensitizer **FBC**, and further evaluated as a remote controllable free radical generation platform for enhancing antitumor efficiency. The **PI/FBC** radical nanogenerator can be excited by NIR light to produce ROS through transfer of energy to oxygen and induce the formation of toxic iodine radicals *via* electron transfer to **PI**. Notably, unlike conventional tumor treatments, such a radical nanogenerator is controllable and insusceptible to oxygen concentration. Moreover, benefiting from the strong NIR emission of **FBC**, the distribution of the **PI/FBC** radical nanogenerator can be monitored without incorporating other imaging agents. This **PI/FBC** radical nanogenerator treatment will no doubt broaden the family of antitumor strategies by using non-oxygen radicals, which is significant for reference in the development of promising anticancer agents.

Introduction

Hypoxia is a typical microenvironment feature in most solid tumors, resulting from the imbalance between oxygen supply and demand.[1,2] A hypoxic microenvironment makes cancer cells resistant to cancer treatments, especially for oxygen-consuming therapies, for instance, photodynamic therapy.[3–6] To enhance the therapeutic efficiency, great efforts have been dedicated to overcoming the bottleneck arising from hypoxia,[7] such as increasing the oxygen concentration,[8–10] reducing the oxygen consumption,[11,12] or combining multiple therapeutic methods.[13–20] Nano-delivery systems provide a promising potency in overcoming hypoxia of tumors, but face challenges such as poor repeatability and potentially adverse toxicity.[21,22] Recently, hypoxia-tolerant photosensitizers have provided a powerful tool for hypoxic tumor treatment.[23–26] These photosensitizers could produce toxic reactive oxygen species (ROS) such as superoxide ($O_2^{\bullet-}$), hydroxyl (·OH) and hydroperoxyl ($HO_2^{\bullet}$) through a photo-induced electron transfer mechanism. However, the produced toxic species are related to oxygen, indicating that the photodynamic therapeutic efficiency of these photosensitizers still relies on oxygen concentration although they require much lower oxygen concentration than traditional photosensitizers.[27] To defeat tumor hypoxia, it would be promising to develop an entirely oxygen-independent platform with remote controllable ability.

Oxygen-irrelevant free radicals are also highly reactive species, which have been extensively employed to synthesize compounds and polymers.[28–31] Benefiting from their efficient generation even under a hypoxic environment, radical nanogenerators based on free radical initiators have been developed to overcome tumor hypoxia for amplifying antitumor efficiency.[32–36] Aside from these radical nanogenerators which focus mainly on thermolabile radical generators, production of free radicals *via* a photo-redox reaction may be another promising approach for hypoxic tumor treatment. Photo-induced radical reactions with excellent controllability have been an appealing option for catalytic organic synthesis and controllable polymerization.[37–40] For cancer therapy, Bu and his co-workers developed a ·Cl nano-generator by decorating a SiO_2-coated upconversion nanoparticle (UCNP) with Ag^0/AgCl heterodots outside, in which ·Cl generation can be triggered by the short wavelength emission of the UCNP upon NIR illumination.[41] In consideration of the energy conversion efficiency, it is a great advantage for efficient oxygen-irrelevant radical formation directly *via* a NIR photosensitizer upon illumination.

Herein, we develop a biocompatible free radical nanogenerator (**PI/FBC**) by the co-assembly of iodized block copolymer POEGMA-*b*-PIEMA (**PI**) and tetrafluorophenyl bacteriochlorin (**FBC**) photosensitizer with strong NIR absorbance for hypoxia-irrelevant phototherapy against tumor hypoxia. As shown in Scheme 1, **FBC** as a NIR photosensitizer can not only produce ROS under NIR illumination, but also induce the production of highly cytotoxic iodine free radicals, endowing the **PI/FBC**

Shanghai Key Laboratory of Functional Materials Chemistry, East China University of Science and Technology, 130 Meilong Road, Shanghai 200237, China. E-mail: wazhang@ecust.edu.cn

† Electronic supplementary information (ESI) available. See DOI: 10.1039/d1sc01220g

‡ These authors contributed equally.

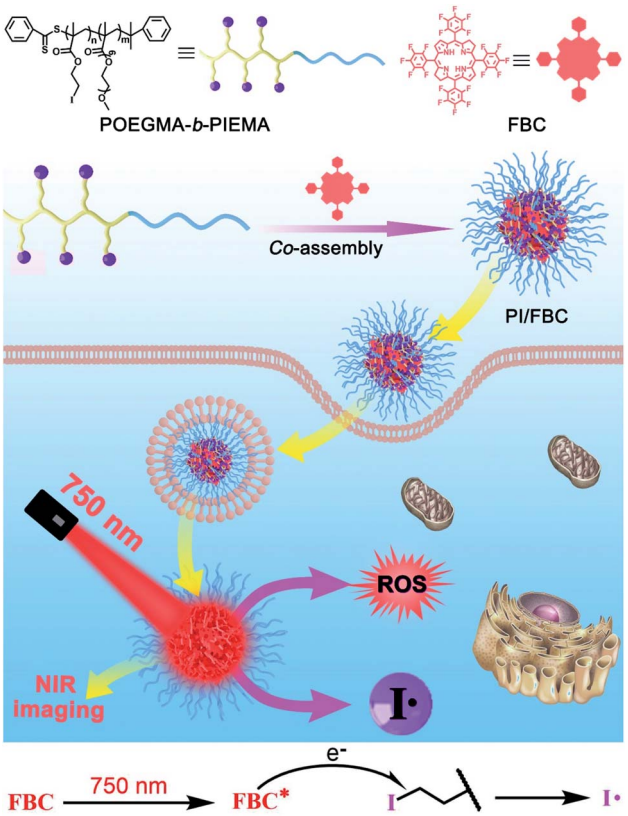

Scheme 1 Preparation of the PI/FBC radical nanogenerator and its antitumor mechanism upon NIR irradiation. Iodine radicals were produced by electron transfer from FBC to PI under NIR irradiation.

nanogenerator with superior remote controllability. Moreover, iodide as the radical initiator was installed on the polymer chain by reversible addition–fragmentation chain transfer (RAFT) polymerization, avoiding unpredictable side effects suffered from the leakage of initiators. Besides, POEGMA as the hydrophilic block can form a hydrophilic shell on the surface of the **PI/FBC** nanogenerator, effectively improving the biocompatibility of the **PI/FBC** radical nanogenerator and extending the circulation time. More importantly, the strong NIR absorption of **FBC** is beneficial to realize deep penetration against skin tissue without severe side effects. Thus, the **PI/FBC** radical nanogenerator may lead to the new trend of free radical-induced tumor therapy, providing a reference for the development of non-oxygen free radicals for future hypoxia antitumor therapy.

Results and discussion

Synthesis of PI/FBC nanoparticles

NIR absorption photosensitizer **FBC** was firstly synthesized according to our previous work (Fig. S1, ESI†).[26] Then, iodine-containing monomer 2-iodoethyl methacrylate was prepared *via* an esterification reaction between methacryloyl chloride and 2-iodoethanol (Fig. S2, ESI†).[42,43] Before POEGMA-*b*-PIEMA was synthesized through RAFT polymerization, a POEGMA macro-RAFT agent was prepared by the homopolymerization of OEGMA according to the route as illustrated in Scheme S1 (ESI†).

The successful synthesis of POEGMA and POEGMA-*b*-PIEMA was confirmed by ^{1}H NMR spectroscopy (Fig. S3 and S4, ESI†) and gel permeation chromatography (GPC, Fig. S5, ESI†), respectively. Afterwards, **PI/FBC** nanoparticles were fabricated by the co-assembly of POEGMA-*b*-PIEMA and **FBC**. The transmission electron microscopy (TEM) image shown in Fig. 1a reveals the well-defined spherical morphology of **PI/FBC** nanoparticles. The hydrodynamic size distribution of **PI/FBC** nanoparticles was determined by dynamic lighting scattering (DLS, Fig. 1b). Compared with **PI** nanoparticles (directly formed by the self-assembly of POEGMA-*b*-PIEMA block polymers), the size of the **PI/FBC** nanoparticles did not increase but decreased slightly after **FBC** was incorporated, which may have resulted from the more concentrated hydrophobic moieties of **FBC**. The zeta potential value of **PI/FBC** nanoparticles was below −10 mV in comparison to that of **PI** nanoparticles, which not only suggested the successful encapsulation of **FBC**, but also showed good colloidal stability as displayed in Fig. 1c. The photophysical properties of **PI/FBC** nanoparticles were evaluated by utilizing UV-vis and fluorescence spectrophotometers (Fig. 1d). The UV-vis spectra of **PI/FBC** nanoparticles indicated that **FBC** was successfully encapsulated in the nanoparticles, in agreement with the DLS and zeta potential results. Besides, owing to the efficient encapsulation of **FBC**, the strong NIR emission of **FBC** can also be observed in the fluorescence spectrum of **PI/FBC** nanoparticles, endowing **PI/FBC** nanoparticles with excellent imaging performance. Additionally, iodine-free **PC/FBC** nanoparticles as the control were prepared by encapsulating **FBC** with a block copolymer, poly(ethylene glycol)-*block*-poly(lactide acid) (PEG-*b*-PLA), and the detailed characterization is shown in Fig. S6–S8 (ESI†).

Reactive species production of PI/FBC nanoparticles

PI/FBC nanoparticles were expected to produce both reactive oxygen species and iodine free radicals upon NIR illumination

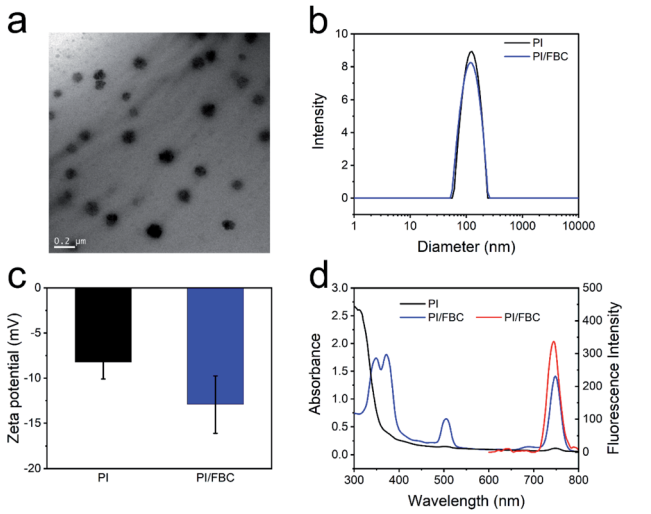

Fig. 1 Characterization of the prepared nanoparticles. (a) Representative TEM image of PI/FBC nanoparticles. (b) Size distribution of nanoparticles determined by dynamic light scattering. (c) Zeta potential of PI and PI/FBC nanoparticles. (d) UV-vis absorption and fluorescence spectra of PI/FBC nanoparticles.

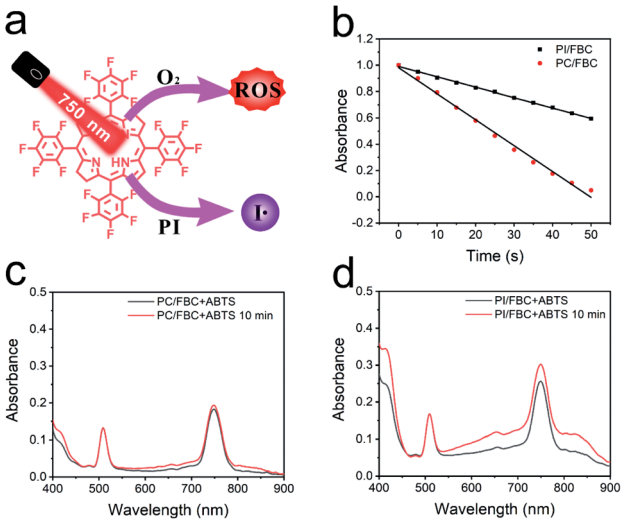

Fig. 2 *In vitro* reactive species production. (a) Illustration of the generation mechanism of reactive species. (b) Changes in the absorption of DPBF at 425 nm induced by **PC/FBC** and **PI/FBC** nanoparticles under illumination. Free radical production of (c) **PC/FBC** and (d) **PI/FBC** nanoparticles determined by using ABTS as a radical probe, respectively.

(Fig. 2a). And then we determined the extracellular reactive species (RS) production of **PI/FBC** nanoparticles before *in vitro* antitumor performance. DPBF as a total ROS probe was employed to measure the ROS production of **PI/FBC** nanoparticles under NIR irradiation.[44] As shown in Fig. 2b, S9 and S10 (ESI†), **PI/FBC** and **PC/FBC** nanoparticles can both cause the absorbance decrease of DPBF with the irradiation time extension, indicating that a significant amount of ROS was generated by the nanoparticles. It is noteworthy that the absorbance decrease of DPBF of **PI/FBC** nanoparticles was modest compared to that of **PC/FBC** nanoparticles, which may be induced by the iodine free radical production of **PI/FBC** nanoparticles. The iodine free radical production competes with the ROS generation to consume excited photosensitizers, resulting in the decrease of ROS formation. To verify the hypothesis, 2,2′-amino-di(2-ethyl-benzothiazoline sulphonic acid-6) ammonium salt (ABTS) as a radical probe was adopted to determine the production of iodine free radicals.[35] We can observe that the UV-vis spectrum of ABTS of **PC/FBC** nanoparticles changed slightly after NIR illumination (Fig. 2c); however, a significant increase was found in that of **PI/FBC** nanoparticles, indicating that a mass of iodine radicals was produced by **PI/FBC** nanoparticles (Fig. 2d). To further confirm the production of free radicals, we also used a radical trapping agent, TEMPO, to capture the produced iodine free radical under NIR illumination (Fig. S11, ESI†). The peak at 2.8 ppm increased with irradiation time extension, suggesting the successful formation of iodine radicals.

Intracellular uptake and photoactivity

Encouraged by the exciting extracellular consequence, *in vitro* antitumor performance was evaluated on 4T1 cells. A confocal laser scanning microscope (CLSM) was employed to determine the cellular internalization and cytotoxic species production of nanoparticles. As shown in Fig. 3a, bright red fluorescence can be observed around the cell nucleus (blue fluorescence), indicating that nanoparticles can efficiently enter cancer cells. Subsequently, 2,7-dichlorofluorescein diacetate (DCFH-DA), a fluorescent probe, was used to determine the production of oxidizing toxic species as shown in Fig. 3b. Compared to **PI** and **PC/FBC** nanoparticles, strong green fluorescence of DCF generated *via* oxidation of reactive species to DCFH-DA was

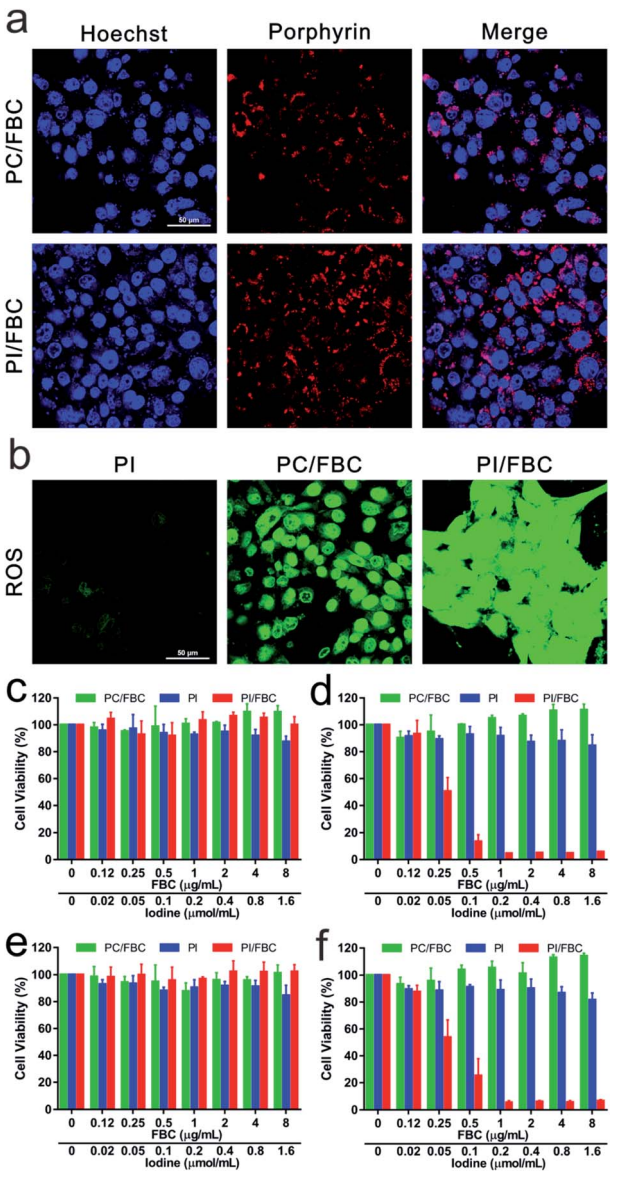

Fig. 3 *In vitro* antitumor performance. (a) Cellular uptake of **PI/FBC** and **PC/FBC** nanoparticles measured using a confocal laser scanning microscope (scale bar: 50 μm). (b) CLSM images of intracellular reactive species (RS) induced by **PI/FBC** and **PC/FBC** nanoparticles (scale bar: 50 μm). (c–f) Relative viabilities of 4T1 cells incubated with a series of concentrations of **PI/FBC** and **PC/FBC** nanoparticles. (c) Dark toxicity and (d) phototoxicity under normoxic conditions. (e) Dark toxicity and (f) phototoxicity under hypoxic conditions (750 nm, 50 mW cm^{-2}, 10 min).

detected after treatment with NIR irradiation in the presence of **PI/FBC** nanoparticles, indicating that the DCF formation resulted from the toxic species produced by **PI/FBC** nanoparticles after NIR irradiation. There was almost no green fluorescence in **PI** nanoparticle treated cells with NIR illumination, which may reveal that **PI** nanoparticles are biocompatible.

MTT assay was employed to further evaluate the antitumor efficiency under normal and hypoxic conditions (**FBC** concentration: 0–8 μg mL^{-1}) (Fig. 3c–f). From Fig. 3c and e, it can be observed that there is no significant cytotoxicity against cells for **PI**, **PC/FBC** and **PI/FBC** nanoparticles, indicating that all the nanoparticles have good biocompatibility. It is noteworthy that, with NIR irradiation (750 nm, 50 mW cm^{-2}, 10 min), **PI/FBC** nanoparticles could efficiently induce cell death in a concentration-dependent manner, even in a hypoxic environment (Fig. 3d and f). However, the **PC/FBC** and **PI** nanoparticle treated cells did not end their days obviously. These results may be associated with the modest or disabled production of toxic species of **PC/FBC** or **PI** nanoparticles, respectively, which is in line with the foregoing consequence of intracellular DCF fluorescence detected by CLSM. In addition, we also determined the cytotoxicity of **PC/FBC** nanoparticles at a higher **FBC** concentration (0–32 μg mL^{-1}) under an elevated laser power density (100 mW cm^{-2}, 15 min) (Fig. S12, ESI†). The results revealed that the cell survival decreased with the increase of **PC/FBC** concentration, which further confirmed that the high cell survival of **PC/FBC** in the previous experiment resulted from the limited ROS generation.

In vivo imaging and biodistribution, photodynamic therapy and bio-safety

Based on the remarkable *in vitro* photo-induced toxicity against cancer cells, an *in vivo* performance study was carried out on nude mice bearing tumors. 4T1 tumor-bearing mice were obtained by subcutaneously injecting 200 μL of 5×10^6 tumor cells. For *in vivo* distribution monitoring *via* fluorescence imaging, **PI/FBC** nanoparticles were injected into mice *via* the tail vein after the xenograft tumor volume reached 100 mm^3. The fluorescence imaging was monitored in real time *via* detecting the emission at 750 nm after **FBC** was excited with 510 nm light. As shown in Fig. 4a and S13 (ESI†), the fluorescence signal at the tumor gradually increased with time extension, suggesting that **PI/FBC** could be efficiently enriched in tumors by the enhanced permeability and retention (EPR) effect of tumors.[45] The biodistribution results also distinctly demonstrated that **PI/FBC** nanoparticles were primarily accumulated in the tumor site 24 h post-injection.

To further verify the antitumor efficiency of **PI/FBC** nanoparticles, mice bearing 4T1 tumors were randomly divided into seven groups (control, **PI**, **PC/FBC**, **PI/FBC**, **PI + L**, **PC/FBC + L** and **PI/FBC + L**) and separately administered with the corresponding nanoparticles through the tail vein when the tumor volume reached 100 mm^3. Tumors in **PI + L**, **PC/FBC + L** and **PI/FBC + L** groups were irradiated with a 750 nm laser for 15 min at a power density of 200 mW cm^{-2}. Tumor volumes and body weights were recorded to evaluate the tumor suppression effect and biocompatibility of nanoparticles, respectively (Fig. 4b and c). We found that **PC/FBC** and **PI/FBC** nanoparticles could significantly inhibit the tumor growth after illumination with a 750 nm laser. It is noteworthy that **PI/FBC** exhibited a superior inhibition efficiency than **PC/FBC**, which could be attributed to the oxygen-irrelevant iodine free radicals generated by **PI/FBC** nanoparticles under illumination. However, **PI** nanoparticles did not show any antitumor effect, indicating that the oxygen-irrelevant free radical production was triggered by **FBC** under 750 nm laser irradiation. Without laser illumination, **PI**, **PC/FBC** and **PI/FBC** nanoparticles all showed no obvious difference compared to the control, revealing that they had a good biocompatibility. No significant weight loss was observed in Fig. 4c, suggesting minimal side effects of the nanoparticles. On 15th day, the mice were sacrificed to harvest tumors and primary organs (heart, liver, spleen, lungs and kidneys) for further evaluation of antitumor efficiency. Isolated tumors were weighed and photographed as depicted in Fig. 4d and e. **PI/FBC + L** treated tumors had the lightest weight and smallest volume, indicating that **PI/FBC** nanoparticles could efficiently inhibit the tumor growth after illumination with a 750 nm laser. H&E

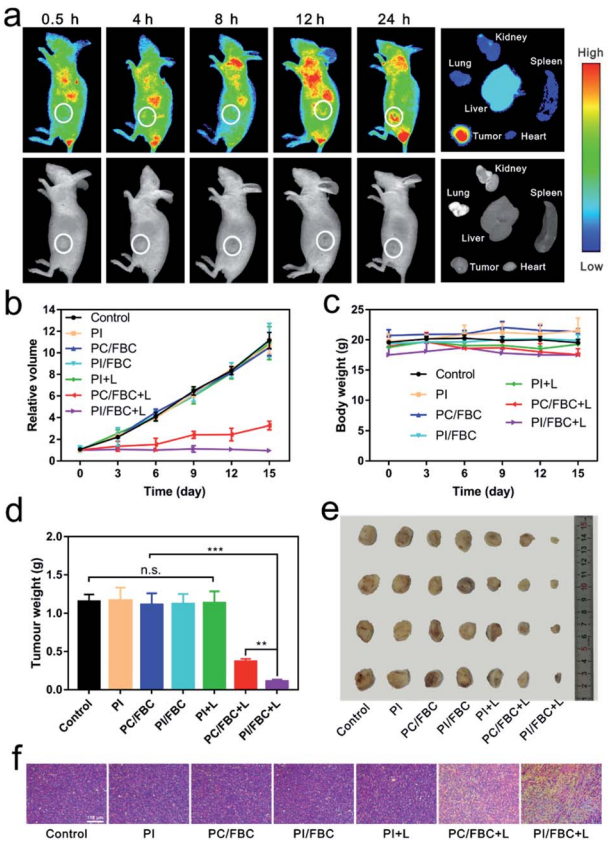

Fig. 4 *In vivo* photo-induced inhibition test against the 4T1 tumor. (a) Changes of *in vivo* distribution of **PI/FBC** nanoparticles with the time extension monitored by fluorescence imaging. (b) Relative tumor volume and (c) the mice body weight during treatment. (d) Tumor weights and (e) photograph of isolated tumors after 15 days of treatment ($n = 4$). (f) Images of a tumor section stained with H&E (scale bar: 150 μm, $^*P < 0.05$, $^{**}P < 0.01$, and $^{***}P < 0.001$).

staining on tissue sections (Fig. 4f and S14, ESI†) also revealed that **PI/FBC** nanoparticles are highly biocompatible with major organs and could cause significant cell necrosis after being triggered by 750 nm laser irradiation.

Conclusions

In conclusion, a biocompatible hypoxia-tolerant nano-system, **PI/FBC**, was fabricated by co-assembling an iodized polymer with a NIR photosensitiser, **FBC**. **PI/FBC** nanoparticles could efficiently accumulate in tumor sites through the EPR effect, which can be monitored in real time *via* NIR fluorescence imaging. Upon being excited with an NIR laser, **PI/FBC** nanoparticles could not only produce cytotoxic ROS by transferring energy to oxygen, but also cause highly toxic iodine free radical production through an oxygen-irrelevant mechanism. Therefore, **PI/FBC** nanoparticles could facilitate a significantly enhanced antitumor efficiency by conquering the hypoxic tumor environment in a controllable manner. This **PI/FBC** radical nanogenerator treatment will no doubt broaden the family of antitumor strategies by using nonoxygen free radicals, which is significant for reference in the development of prospective anticancer agents.

Data availability

The electronic supplementary information include experimental detail, NMR data, spectra data and histological data.

Author contributions

Z. Liu conceived the project and designed the experiments. Z. liu and M. Wu performed the sample preparation, characterization and biological experiment. Z. Liu and M. Wu wrote the paper and contributed equally. All authors discussed the results and commented on the manuscript.

Ethical statement

All animal studies were conducted on male Balb/c nude mice (four to five weeks) in compliance with the National Institutes of Health Guide for the Care and Use of Laboratory Animals approved by the Animal Care and Use Committee of East China University of Science and Technology.

Conflicts of interest

There are no conflicts to declare.

Acknowledgements

This work was financially supported by the National Natural Science Foundation of China (No. 22075079 and 21875063) and the Science and Technology Commission of Shanghai Municipality for the Shanghai International Cooperation Program (19440710600).

References

1 W. R. Wilson and M. P. Hay, *Nat. Rev. Cancer*, 2011, **11**, 393–410.
2 J. M. Brown and W. R. Wilson, *Nat. Rev. Cancer*, 2004, **4**, 437–447.
3 T. M. Ashton, E. Fokas, L. A. Kunz-Schughart, L. K. Folkes, S. Anbalagan, M. Huether, C. J. Kelly, G. Pirovano, F. M. Buffa, E. M. Hammond, M. Stratford, R. J. Muschel, G. S. Higgins and W. G. McKenna, *Nat. Commun.*, 2016, **7**, 12308.
4 K. Graham and E. Unger, *Int. J. Nanomed.*, 2018, **13**, 6049–6058.
5 X. Jing, F. Yang, C. Shao, K. Wei, M. Xie, H. Shen and Y. Shu, *Mol. Cancer*, 2019, **18**, 157.
6 A. Sahu, I. Kwon and G. Tae, *Biomaterials*, 2020, **228**, 119578.
7 C. D. Phung, T. H. Tran, L. M. Pham, H. T. Nguyen, J. H. Jeong, C. S. Yong and J. O. Kim, *J. Controlled Release*, 2020, **324**, 413–429.
8 S. C. Zhang, Q. Z. Li, N. Yang, Y. H. Shi, W. Ge, W. J. Wang, W. Huang, X. J. Song and X. C. Dong, *Adv. Funct. Mater.*, 2019, **29**, 1906805.
9 L. Xing, J. H. Gong, Y. Wang, Y. Zhu, Z. J. Huang, J. Zhao, F. Li, J. H. Wang, H. Wen and H. L. Jiang, *Biomaterials*, 2019, **206**, 170–182.
10 Z. Liu, Y. Xue, M. Wu, G. Yang, M. Lan and W. Zhang, *Biomacromolecules*, 2019, **20**, 4563–4573.
11 W. Lv, Z. Zhang, K. Y. Zhang, H. Yang, S. Liu, A. Xu, S. Guo, Q. Zhao and W. Huang, *Angew. Chem., Int. Ed.*, 2016, **55**, 9947–9951.
12 M. Li, Y. Shao, J. H. Kim, Z. Pu, X. Zhao, H. Huang, T. Xiong, Y. Kang, G. Li, K. Shao, J. Fan, J. W. Foley, J. S. Kim and X. Peng, *J. Am. Chem. Soc.*, 2020, **142**, 5380–5388.
13 L. H. Fu, C. Qi, Y. R. Hu, J. Lin and P. Huang, *Adv. Mater.*, 2019, **31**, 1808325.
14 D. Cui, J. Huang, X. Zhen, J. Li, Y. Jiang and K. Pu, *Angew. Chem., Int. Ed.*, 2019, **58**, 5920–5924.
15 X. Zhao, S. Long, M. Li, J. Cao, Y. Li, L. Guo, W. Sun, J. Du, J. Fan and X. Peng, *J. Am. Chem. Soc.*, 2020, **142**, 1510–1517.
16 Y. Jiang, X. Zhao, J. Huang, J. Li, P. K. Upputuri, H. Sun, X. Han, M. Pramanik, Y. Miao, H. Duan, K. Pu and R. Zhang, *Nat. Commun.*, 2020, **11**, 1857.
17 Y. Jiang, J. Li, Z. Zeng, C. Xie, Y. Lyu and K. Pu, *Angew. Chem., Int. Ed.*, 2019, **58**, 8161–8165.
18 J. Li, D. Cui, Y. Jiang, J. Huang, P. Cheng and K. Pu, *Adv. Mater.*, 2019, **31**, 1905091.
19 Z. Zeng, C. Zhang, J. Li, D. Cui, Y. Jiang and K. Pu, *Adv. Mater.*, 2021, **33**, 2007247.
20 S. He, Y. Jiang, J. Li and K. Pu, *Angew. Chem., Int. Ed.*, 2020, **59**, 10633–10638.
21 K. Cho, X. Wang, S. Nie, Z. G. Chen and D. M. Shin, *Clin. Cancer Res.*, 2008, **14**, 1310–1316.
22 D. Sun, S. Zhou and W. Gao, *ACS Nano*, 2020, **14**, 12281–12290.
23 T. Luo, K. Ni, A. Culbert, G. Lan, Z. Li, X. Jiang, M. Kaufmann and W. Lin, *J. Am. Chem. Soc.*, 2020, **142**, 7334–7339.

24 K. Zhang, Z. Yu, X. Meng, W. Zhao, Z. Shi, Z. Yang, H. Dong and X. Zhang, *Adv. Sci.*, 2019, **6**, 1900530.
25 L. Li, C. Shao, T. Liu, Z. Chao, H. Chen, F. Xiao, H. He, Z. Wei, Y. Zhu, H. Wang, X. Zhang, Y. Wen, B. Yang, F. He and L. Tian, *Adv. Mater.*, 2020, **32**, 2003471.
26 M. Wu, Z. Liu and W. Zhang, *Chem. Sci.*, 2021, **12**, 1295–1301.
27 S. Kuang, L. Sun, X. Zhang, X. Liao, T. W. Rees, L. Zeng, Y. Chen, X. Zhang, L. Ji and H. Chao, *Angew. Chem., Int. Ed.*, 2020, **59**, 20697–20703.
28 M. J. Black, K. F. Biegasiewicz, A. J. Meichan, D. G. Oblinsky, B. Kudisch, G. D. Scholes and T. K. Hyster, *Nat. Chem.*, 2020, **12**, 71–75.
29 J. Sinha, B. D. Fairbanks, H. B. Song and C. N. Bowman, *ACS Macro Lett.*, 2019, **8**, 213–217.
30 P. Li, J. Zhao, L. Shi, J. Wang, X. Shi and F. Li, *Nat. Commun.*, 2018, **9**, 1972.
31 J. Han and J. Xie, *Chem*, 2020, **6**, 1053–1055.
32 X. Q. Wang, F. Gao and X. Z. Zhang, *Angew. Chem., Int. Ed.*, 2017, **56**, 9029–9033.
33 S. Shen, C. Zhu, D. Huo, M. Yang, J. Xue and Y. Xia, *Angew. Chem., Int. Ed.*, 2017, **56**, 8801–8804.
34 X. M. Li, Y. Liu, F. Fu, M. B. Cheng, Y. T. Liu, L. C. Yu, W. Wang, Y. D. Wan and Z. Yuan, *Nano-Micro Lett.*, 2019, **11**, 68.
35 H. Xiang, H. Lin, L. Yu and Y. Chen, *ACS Nano*, 2019, **13**, 2223–2235.
36 Y. P. Wan, G. H. Lu, J. F. Zhang, Z. Y. Wang, X. Z. Li, R. Chen, X. Cui, Z. M. Huang, Y. F. Xiao, J. Chelora, W. J. Zhang, Y. H. Liu, M. Li, H. Y. Xie and C. S. Lee, *Adv. Funct. Mater.*, 2019, **29**, 1903436.
37 L. Wang, J. M. Lear, S. M. Rafferty, S. C. Fosu and D. A. Nagib, *Science*, 2018, **362**, 225–229.
38 M. C. Fu, R. Shang, B. Zhao, B. Wang and Y. Fu, *Science*, 2019, **363**, 1429–1434.
39 A. E. Bosnidou and K. Muniz, *Angew. Chem., Int. Ed.*, 2019, **58**, 7485–7489.
40 H. L. Cao, G. C. Wang, Y. D. Xue, G. L. Yang, J. Tian, F. Liu and W. A. Zhang, *ACS Macro Lett.*, 2019, **8**, 616–622.
41 R. Song, H. Wang, M. Zhang, Y. Liu, X. Meng, S. Zhai, C. C. Wang, T. Gong, Y. Wu, X. Jiang and W. Bu, *Angew. Chem., Int. Ed.*, 2020, **59**, 21032–21040.
42 Y. H. Chang, P. Y. Lin, M. S. Wu and K. F. Lin, *Polymer*, 2012, **53**, 2008–2014.
43 G. Amitai, H. Murata, J. D. Andersen, R. R. Koepsel and A. J. Russell, *Biomaterials*, 2010, **31**, 4417–4425.
44 T. Entradas, S. Waldron and M. Volk, *J. Photochem. Photobiol., B*, 2020, **204**, 111787.
45 D. Peer, J. M. Karp, S. Hong, O. C. Farokhzad, R. Margalit and R. Langer, *Nat. Nanotechnol.*, 2007, **2**, 751–760.